LAWRENCE
LIVERMORE
NATIONAL
LABORATORY

UCRL-CONF-225607

LX-17 Deflagration at High Pressures and Temperatures

Jake Koerner, Jon Maienschein, Kevin Black, Martin DeHaven, Jeff Wardell

October 25, 2006

Joint Army-Navy-NASA-Air Force 41st Combustion, 29th Airbreathing Propulsion, 23rd Propulsion Systems Hazards Joint Subcommittee Meeting
San Diego, CA, United States
December 4, 2006 through December 8, 2006

LX-17 DEFLAGRATION AT HIGH PRESSURES AND TEMPERATURES*

J. Koerner, J. Maienschein, K. Black, M. DeHaven, J. Wardell
Lawrence Livermore National Laboratory Energetic Materials Center
Livermore, CA

ABSTRACT

We measure the laminar deflagration rate of LX-17 (92.5 wt% TATB, 7.5 wt% Kel-F 800) at high pressure and temperature in a strand burner, thereby obtaining reaction rate data for prediction of thermal explosion violence. Simultaneous measurements of flame front time-of-arrival and temporal pressure history allow for the direct calculation of deflagration rate as a function of pressure. Additionally, deflagrating surface areas are calculated in order to provide quantitative insight into the dynamic surface structure during deflagration and its relationship to explosion violence. Deflagration rate data show that LX-17 burns in a smooth fashion at ambient temperature and is represented by the burn rate equation $B = 0.2P^{0.9}$. At 225 °C, deflagration is more rapid and erratic. Dynamic deflagrating surface area calculations show that ambient temperature LX-17 deflagrating surface areas remain near unity over the pressure range studied.

INTRODUCTION

During the response of energetic materials to hazards such as thermal or mechanical stimuli, the initial low-level reaction releases sufficient energy to cause an increase in pressure and temperature that leads to acceleration of reaction until a runaway condition is reached. Accurate knowledge of reaction rates at conditions typical of those in accelerating reactions is necessary to understand and predict the violence of the ensuing explosion.

For explosives and propellants undergoing thermal explosion or mechanical impact, hydrodynamic calculations show pressures in the reacting material of several hundred MPa (several kbar) and higher. Therefore, laminar deflagration rate measurements and deflagrating surface area calculations of these materials at high pressures and temperatures are needed for accurate prediction of reaction violence through computer simulation.[1,2]

EXPERIMENTS AND CALCULATIONS

LLNL HIGH PRESSURE STRAND BURNER

The LLNL High Pressure Strand Burner, shown schematically in Figure 1, combines the features of a traditional closed-bomb burner with those of a traditional strand burner. It contains a deflagrating sample in a small volume, high-pressure chamber. Simultaneous temporal pressure and burn front time-of-arrival measurements yield the laminar deflagration rate for a range of pressures and provide insight into deflagration uniformity in one experiment. Pressure is measured using a pressure transducer and a load cell, and burn front arrival is detected by the burning-through of thin silver wires embedded in the sample. High speed digital scopes capture the data for subsequent analysis.

The strand burner has an internal volume of approximately 75 cm^3 (4.6 in^3) and is designed to reach pressures of 1 GPa (150,000 psi). The pressure vessel body is built from two concentric shells with interference between them to put the inner shell in compression. The standard inner liner and the top and bottom closures are fabricated from hardened S-5 tool steel, which is high strength but also brittle and prone to corrosion. The S-5 tool steel is suitable for experiments with LX-17 which generates little or no corrosive gasses. The top end plug is equipped with gas inlet and outlet ports and a pressure transducer,

*This work was performed under the auspices of the U.S. Department of Energy by University of California, Lawrence Livermore National Laboratory under contract W-7405-Eng-48.

while the bottom end plug holds a prewired base and high pressure feed-throughs for the burn wires, igniter wires, and thermocouples. The pressure transducer is a Kistler model 6213B. The load cell is Omega model LCTB-150K. The commercial sensor was calibrated to NIST standards by the manufacturer, and the load cell was calibrated against the Kistler transducer.

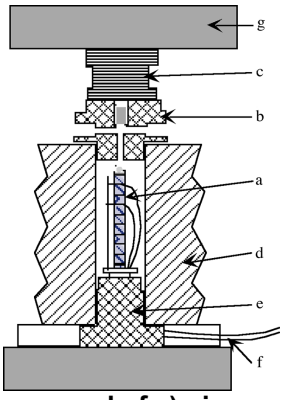

Figure 1. Strand burner schematic composed of a) nine segment burn sample with burn wires evenly spaced between segments (only two wires shown for clarity) and igniter on top, b) top plug with inlet and outlet ports and pressure transducer in center, c) load cell, d) pressure vessel, e) bottom plug with wire feed-throughs, f) signal wires to electronics, g) load frame (top and bottom).

The burn sample, shown in Figure 2, consists of nine 6.35 mm (0.25 in) length by 6.35 mm diameter cylinders stacked on end. Seventy-five micron (3 mil) diameter silver burn wires are inserted radially in a groove between each pair of pellets. After assembly, the cylindrical surface of the sample is coated with epoxy to inhibit burning on that surface. This limits the flame front to the cross-sectional surface of the cylinder. An igniter train consisting of an igniter wire, approximately 110 mg of B/KNO_3, and a thin, 30 mg pressed HNS pellet ignites the burn sample on the top end of the cylinder. Further details are available in the literature.[3]

Figure 2. Sample holder and explosive sample. Burn wires are inserted through holes in Teflon® tube into sample. B/KNO_3 and HNS igniter and cardboard tube is on top, with igniter wires leading to it. Thermocouple in front is used to monitor temperature inside pressure vessel.

To conduct a measurement, the sample is mounted into a pre-wired base that carries the signal wires through high pressure feed-throughs in the bottom plug of the pressure vessel. The sample and bottom plug are then inserted into the pressure vessel. The system is pressurized to the desired starting pressure (up to 400 MPa or 60,000 psi) with argon and remotely sealed by immersing the inlet and outlet argon gas lines in liquid nitrogen. The argon freezes and acts as a remotely actuated pressure isolation valve with no moving parts or seals to maintain. Once the desired pressure is reached, sample deflagration is initiated, and temporal pressure and burn front time-of-arrival data are recorded. Following the run, the pressure is released by remotely removing the outlet argon gas line from the liquid nitrogen.

Typical pressure and flame front time-of-arrival data are shown in Figure 3.

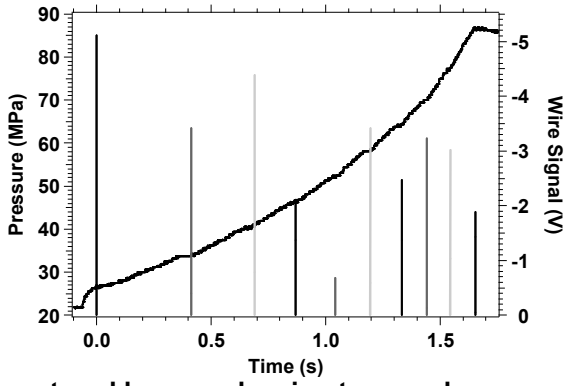

Figure 2. Typical data from strand burner, showing temporal pressure behavior and flame-front time-of-arrival signals. Each time-of-arrival signal has unique identifier. Wires 1 (at ignitor), 4, 7, and 10 – black line; wires 2, 5, 8 – dark grey line; wires 3, 6, 9 – light gray line. Each set has first wire set at maximum amplitude, second wire at minimum amplitude, and third wire at intermediate amplitude.

The burn wire electronics provide a well defined signal, with measured rise times less than 40 microseconds. The wires burn through reproducibly, with wires mounted at the same location in the sample showing a standard deviation of 1-2 milliseconds. The wires do take several milliseconds to burn through; however, this time is essentially independent of initial pressure and temperature conditions and therefore does not affect the deflagration rate calculation by differences in time-of-arrival. The burn wire at the bottom of the stack does not burn through unless enough energetic material is placed below it to provide several milliseconds of burning once the flame front has passed. Burn wires are recorded in a way which allows for unambiguous assignment of each signal to a particular wire. This is necessary, as wires occasionally report out of sequence if broken by debris in the bomb chamber.

The burn wire data should cover the time span of the pressure signal. Any significant deviation form this indicates anomalous behavior. For example, the report of all burn wires before the pressure reaches a maximum indicates that the deflagration front passes rapidly down the sample and leaves still-reacting material behind. This behavior is indicative of flame spread through the sample or of propagation of the flame down the side of the sample; however, the epoxy coating should inhibit the latter.

To calculate deflagration rate as a function of pressure, the length and time-of-arrival for each pair of pellets is used, and the corresponding average pressure for this segment of the sample is calculated. The temporal pressure data can be used to calculate vivacity and surface area.[4,5,9]

MATERIALS

The LX-17 used is 92.5 ± 0.3 wt% water-aminated TATB and 7.5 ± 0.3 wt% Kel-F 800. At least 50 wt% of the virgin TATB particles are smaller than 20 microns, and at least 75 wt% are smaller than 45 microns. Kel-F 800 specifications conform to Los Alamos National Laboratory Specification Number 13Y-188481. Additional formulation details can be found in the Lawrence Livermore National Laboratory (LLNL) specification, “LX-17 High Explosive Molding Powder - RM255117”.

LX-17 was uniaxially pressed in a mechanical pressing die at 207 MPa (30,000 psi) and 105 °C (221 °F). The LLNL lot identification number is C-329.

CALCULATIONS

Reactions taking place during the final explosion are, in situations that do not involve shock stimuli, deflagrative in nature. Therefore, measurement of deflagration rate at high pressures and temperatures provides necessary information on runaway reaction behavior. This information is summarized in the burn rate equation,

$$B = aP^n \tag{1}$$

where B is the burn rate (mm/s), a is the burn rate coefficient (mm/s·MPa^n), P is the pressure (MPa) and n is the burn rate coefficient (dimensionless).

Additionally, an equation which follows a well known vivacity concept in combustion aids in quantifying the change in sample surface area available for deflagration and provides insight into overall explosion violence. This equation,

$$\frac{S}{S_o} = \left(\frac{1}{P^n}\frac{dP}{dt}\right)\frac{L}{a(P_f - P_o)} \tag{2}$$

is used to help characterize deflagration as either laminar or as "flame-spread" by calculating the deflagrating surface area, S, and normalizing it to the laminar deflagrating surface area, S_o, which is also the cross sectional area of the strand.[9] Written this way, laminar deflagration ($S/S_o \approx 1$) and flame-spread deflagration ($S/S_o >> 1$) regimes are more easily observed.

In Equation 2, the variable, P, is the time dependent chamber pressure (MPa), the constant, L, is the length (mm) of the deflagrating strand at t = 0, and the constants a and n are the burn rate parameters obtained from Equation 1. P_f and P_o are final and initial chamber pressure (MPa), respectively.

RESULTS AND DISCUSSION

DEFLAGRATION RATE MEASUREMENTS

Deflagration rate measurements were conduced at ambient and elevated temperatures. In both cases, deflagration rates were calculated from burn wire data. Burn wire data from ambient temperature runs are smooth and uniform; however, burn wire data from elevated temperature runs were often erratic. Therefore, deflagration rates based on burn wire data from elevated temperature runs should be interpreted with caution. An example of one run is shown in Figure 4.

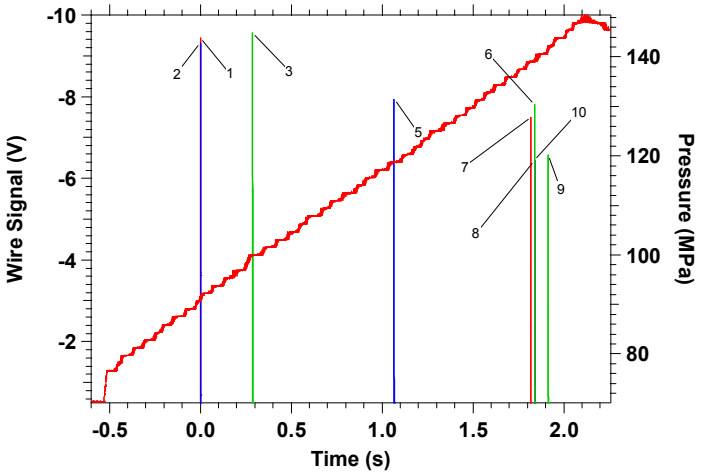

Figure 4. Elevated temperature LX-17 burn wire data illustrating erratic wire reports.

In Figure 4, burn wires report early, late, and out of order. Flying debris in the bomb chamber or flames spreading through the unreacted material ahead of the burn front can cause early reporting of burn wires. These data make burn wire interpretation and subsequent calculation of deflagration rates particularly challenging. So, an overall deflagration rate based on the final and initial pressure, and not on burn wire data, is also calculated as follows:

$$\left\{\begin{array}{c}\text{deflagrati on rate based on}\\ \text{final and initial pressure}\end{array}\right\} = \frac{\left\{\begin{array}{c}\text{total length}\\ \text{of strand}\end{array}\right\}}{\left\{\begin{array}{c}\text{time at which pressure}\\ \text{stops inceasing}\end{array}\right\} - \left\{\begin{array}{c}\text{time at which pressure}\\ \text{starts increasing}\end{array}\right\}} \quad (3)$$

The corresponding average pressure from the run is also calculated and paired with the result of Equation 3. This datum provides a check against the burn wire data; however, it should also be interpreted carefully. We assume that only laminar burn occurs, which is analogous to assuming that there is no flame spread through pores or defects in the sample ahead of the flame front. Data from Figure 4 suggest that flame spread may occur, as the burn wires report before the pressure reaches a maximum (i.e. before LX-17 has finished deflagrating). If flame spread does occur, the calculated burn rate datum from Equation 3 is falsely high.

LX-17 deflagration rate data are shown in Figure 5. Deflagration rate data from runs conducted at ambient temperature are shown as closed, disconnected circles. Deflagration rate data from each run conducted at 225 °C (437 °F) are shown as a closed, connected symbol set. The corresponding burn rate datum based on final and initial pressure measurements (Equation 3) is shown as a matching open symbol.

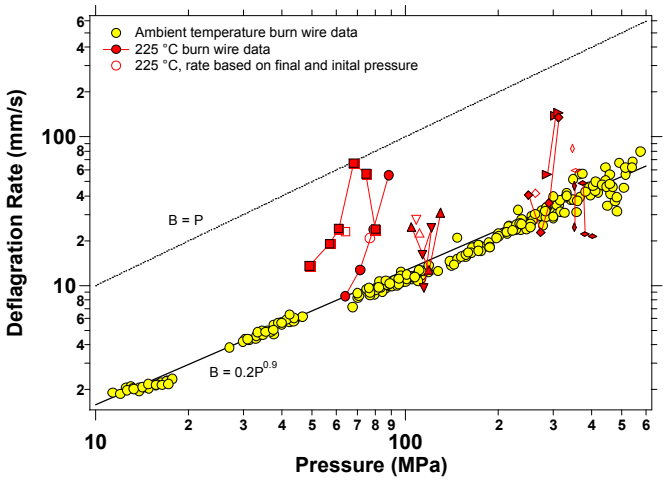

Figure 5. LX-17 deflagration rate data for ambient and elevated temperature runs.

The best fit to the ambient temperature deflagration rate data shown in Figure 5 is $B = 0.2P^{0.9}$. The burn rate equation B = P, which represents the deflagration behavior of some HMX-based explosives (e.g. LX-04) is also plotted for comparison.[3]

Deflagration rates of heated samples are up to an order of magnitude higher than deflagration rates of ambient temperature samples. On average, the deflagration rates of heated samples are approximately twice as fast as those of ambient temperature samples. The increase may be caused by either a physical or a chemical change in the sample. Axial and radial dimensional changes of approximately 3.6 and 2.4 percent, respectively, were observed in cylindrical LX-17 samples heated to 225 °C, respectively.[6] This volumetric expansion may create voids in the sample through which flames can propagate, leading to flame spread through the sample, erratic reporting of burn wires, and rapid deflagration rates. Alternatively, heating may cause a chemical change in the sample, leading to

increased deflagration rates. A basic analysis using the Arrhenius Equation illustrates this and is shown below.

$$\frac{k_2}{k_1} = \exp\left(-\frac{E_a}{R}\left(\frac{1}{T_2}-\frac{1}{T_1}\right)\right) = \exp\left(-\frac{251000}{8.314}\left(\frac{1}{2625}-\frac{1}{2425}\right)\right) = 2.6$$

In this example, k is the rate constant (m^3/mol·s), E_a is the activation energy of TATB[7] (J/mol), R is the universal gas constant (J/mol·K), and T_1 and T_2 are the adiabatic flame temperatures of LX-17[8] (K) at constant volume at 25 and 225 °C, respectively. We see that the rate constant increases by a factor of 2.6 when the temperature increases by 200 °C. This corresponds fairly well with the average of the increased deflagration rates observed for elevated temperature samples.

Regardless of the cause, faster deflagration rates generally lead to increased reaction violence, so it is important to take note of this change.

SURFACE AREA CALCULATIONS

Surface area calculations depend on accurate burn rate parameters from the burn rate equation $B = aP^n$ and on accurate pressure measurements inside the chamber. These calculations show deviation from laminar burn – where the burn front is limited to only the cross-sectional surface of the cylinder.

An example of one particular surface area analysis is shown below in Figure 6.

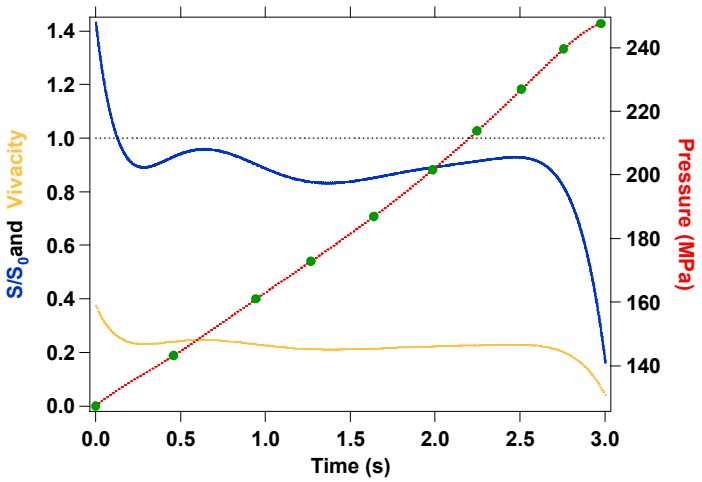

Figure 6. Illustrative surface area analysis example.

Normalized surface area, S/S_o, and vivacity (shown for comparison) are plotted on the left y-axis while pressure is plotted on the right y-axis. The circular symbols represent the time at which each burn wire reports and are analogous to the wire signals shown in Figures 3 and 4. The pressure increase is smooth and the burn wire reports are ordered and evenly spaced. S/S_o remains near unity for the duration of the run. The high surface area at the beginning of the run is attributed to the increase in pressure from the deflagration of the B/KNO_3 and HNS igniter and should be ignored. For subsequent analyses, surface areas near ignition are omitted. The low surface area near the end of the run is attributed to the final consumption of the deflagrating material. As the run ends, the material is depleted, dP/dt decreases, and, consequently, S/S_o decreases.

A summary of surface area calculations are plotted as a function of pressure for ambient temperature runs in Figure 7. For ambient temperature runs, surface area remains near unity.

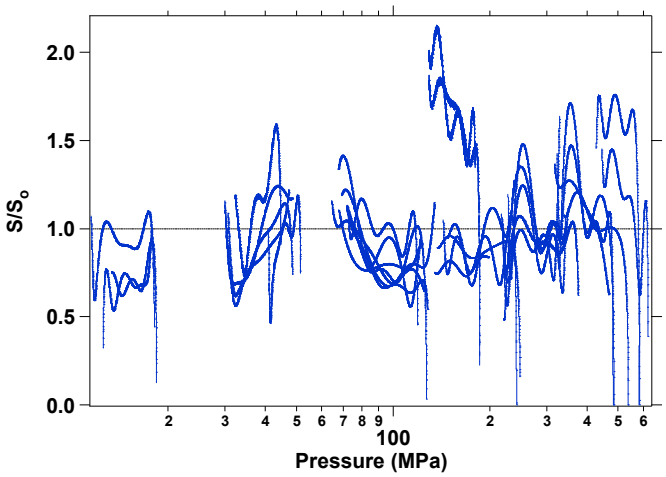

Figure 7. LX-17 normalized surface area data for ambient temperature runs.

Like LX-17, PBXN-109, which is known to deflagrate in a smooth, laminar fashion, shows normalized surface areas near unity over the pressure range studied.[9] In contrast to LX-17, other materials such as C-4 and Composition B, which are known to exhibit greatly increased deflagration rates (based on burn wire data) at particular pressures or at particular times during a run, show increases in normalized surface areas by up to a factor of 80 and 20, respectively.[9] LX-17, with a low pressure dependence on deflagration rate and a low propensity to deconsolidate is expected to show relatively weak violence during a thermal explosion; however, further experimentation is needed to validate this assumption.

The increase in deflagration rate and concomitant increase in pressure during heated runs may be caused by a chemical, and not a physical change in the material. Because the S/S_o calculation reports only a physical change (and not a chemical change) in the material during deflagration, we do not report S/S_o values for heated runs.

SUMMARY AND CONCLUSIONS

We measured the laminar deflagration rate of LX-17 at high pressure and temperature in a strand burner and obtained reaction rate data for prediction of thermal explosion violence. By simultaneously measuring flame front time-of-arrival and temporal pressure history, we calculated the LX-17 deflagration rate as a function of pressure as $B = 0.2P^{0.9}$. Based on the analysis of erratic burn wire data of samples heated to 225 °C , we saw increases in deflagration rates of up to an order of magnitude higher than deflagration rates of ambient temperature runs. On average, deflagration rates of heated runs were about twice as fast as those of ambient temperature runs. Interestingly, LX-17 deflagration rates during heated runs are still slower than deflagration rates of several HMX-based explosives during ambient temperature runs. Overall deflagration rate calculations based on Equation 3 support the burn wire data at elevated temperatures, but have some limitations.

Additionally, we calculated deflagrating surface areas in order to provide quantitative insight into the dynamic surface structure during deflagration. LX-17 normalized surface areas remain near unity over the pressure range studied for ambient temperature samples, indicating that deconsolidation or flame spread is not likely to occur.

ACKNOWLEDGEMENTS

We gratefully acknowledge Sally Weber and Greg Sykora for their contributions to this experimental effort, and Alan Burnham for his insight during discussions as the work progressed.

REFERENCES

1. J.L. Maienschein and J.B. Chandler, ***High Pressure Laminar Burn Rates of AP/Al/HTPB Propellants***, in Proceedings of JANNAF 34th Combustion and 16th Propulsion Systems Hazards Subcommittee Meetings, West Palm Beach, FL, CPIA Publication 657 Volume II, p. 95 (1997).

2. J.L. Maienschein, E.L. Lee, J.E. Reaugh, C.I. Merrill and R.R. Lambert, ***Modeling the Impact Response of Booster Propellants***, in Proceedings of JANNAF 34th Combustion and 16th Propulsion Systems Hazards Subcommittee Meetings, West Palm Beach, FL, CPIA Publication 657, Vol II, p. 163 (1997).

3. J.L. Maienschein, J.F. Wardell, M.R. DeHaven, C.K. Black, ***Deflagration of HMX-Based Explosives at High Temperatures and Pressures***, in Propellants, Explosives, Pyrotechnics 29, No. 5. (2004).

4. A. Birk, D.E. Kooker and P. Baker, ***Model of Cavity Combustion Within an Energetic Solid: Application to Composition-B***, Proceedings of JANNAF 37th Combustion and 19th Propulsion Systems Hazards Subcommittee Meetings, Monterey, CA, CPIA, Publication 704, Vol. II, p. 95 (2000).

5. R. Lieb and P. Baker, ***Combustion Morphology of TNT and Composition B***, Proceedings of JANNAF 37th Combustion and 19th Propulsion Systems Hazards Subcommittee Meetings, Monterey, CA, CPIA, Publication 704, Vol. II, p. 81 (2000).

6. J.L. Maienschein, F. Garcia, ***Thermal Expansion of TATB-based Explosives from 300 to 566 K***, submitted to the Termochimica Acta Journal (May 2001).

7. R.N. Rogers, ***Thermochemistry of Explosives***, Thermochimica Acta Journal, 11, pp. 131–139, (1975).

8. L.E. Fried, K.R. Glaesemann, W.M. Howard, P.C. Souers, P.A. Vitello, ***CHEETAH Thermochemical Code - Calculation of Constant Volume Explosion State***, Version 4.0.

9. J.G. Koerner, J.L. Maienschein, C.K. Black, M.R. DeHaven, ***Laminar and Deconsolidative Deflagration of RDX-based Explosives at High Pressures***, in Proceedings of the 13th International Detonation Symposium, Norfolk, VA, Office of Naval Research (July 2006).